Commun. Comput. Phys.
doi: 10.4208/cicp.101214.250515s

Vol. **18**, No. 4, pp. 957-984
October 2015

Construction, Analysis and Application of Coupled Compact Difference Scheme in Computational Acoustics and Fluid Flow Problems

Jitenjaya Pradhan, Amit, Bikash Mahato, Satish D. Dhandole and Yogesh G. Bhumkar*

School of Mechanical Sciences, Indian Institute of Technology Bhubaneswar, Bhubaneswar, Odisha, India, 751013.

Received 10 December 2014; Accepted (in revised version) 25 May 2015

Abstract. In the present work, a new type of coupled compact difference scheme has been proposed for the solution of computational acoustics and flow problems. The proposed scheme evaluates the first, the second and the fourth derivative terms simultaneously. Derived compact difference scheme has a significant spectral resolution and a physical dispersion relation preserving (DRP) ability over a considerable wavenumber range when a fourth order four stage Runge-Kutta scheme is used for the time integration. Central stencil has been used for the present numerical scheme to evaluate spatial derivative terms. Derived scheme has the capability of adding numerical diffusion adaptively to attenuate spurious high wavenumber oscillations responsible for numerical instabilities. The DRP nature of the proposed scheme across a wider wavenumber range provides accurate results for the model wave equations as well as computational acoustic problems. In addition to the attractive feature of adaptive diffusion, present scheme also helps to control spurious reflections from the domain boundaries and is projected as an alternative to the perfectly matched layer (PML) technique.

AMS subject classifications: 65N06, 65N35, 76D05, 76D17

Key words: Coupled compact difference scheme, DRP property, adaptive numerical diffusion, computational acoustic, PML technique.

1 Introduction

Computational acoustics is an important and active research area [1–5]. Acoustic signals propagate in the form of longitudinal waves in air. Pressure fluctuations associated

*Corresponding author. *Email addresses:* jp10@iitbbs.ac.in (J. Pradhan), am17@iitbbs.ac.in (Amit), bm12@iitbbs.ac.in (B. Mahato), satish@iitbbs.ac.in (S. D. Dhandole), bhumkar@iitbbs.ac.in (Y. G. Bhumkar)

 ©2015 Global-Science Press

https://doi.org/10.4208/cicp.101214.250515s Published online by Cambridge University Press

with acoustic signals are usually very small as compared to the large background pressure field. Effects of viscosity of the medium on the propagation of acoustic signal are negligibly small when the signal propagates over a short distance [6]. Calculations of acoustic problems have to be performed for a long duration avoiding numerical instabilities to obtain spectral contents of the signals [1]. In this context, the chosen discretization schemes should neither numerically amplify nor attenuate the acoustic signal. Propagation of a computed acoustic signal strongly depends on the phase, dissipation and the dispersion properties associated with individual wavenumber component for the used discretization schemes [2, 5, 7]. Hence, the accurate computation of the acoustic field is a challenging topic.

Computational aeroacoustics (CAA) problems are focused on obtaining numerical solution of formation and propagation of acoustic disturbances due to fluctuations in the fluid flow [2, 8, 9]. For an accurate numerical solution, it is necessary that the numerical scheme must resolve all the scales present in the acoustic field as well as flow field. Hence the used numerical scheme must have a higher spectral resolution. In addition, numerical propagation speed of all the resolved scales must be identical to the corresponding physical propagation speed of the individual scale in order to avoid dispersion error [10–14]. It is very much important to ensure that the used numerical scheme is capable of correctly estimating amplitudes and speed of all the fluctuations in the fluid flow which act as an acoustic source. The scheme must exhibit a better DRP nature across a large wavenumber range [12, 14–16] as compared to the traditional discretization schemes.

Compact schemes are widely used for solving computational aeroacoustics problems as well as fluid flow problems [2, 3, 17, 18]. These schemes provide excellent spectral resolution as compared to the traditional explicit discretization methods while evaluation of various derivative terms [5, 17–23]. These schemes have a relatively compact stencil as compared to the traditional explicit schemes of same order and same spectral resolution [14]. In compact schemes, derivative of a function is obtained by either solving a tri-diagonal or a penta-diagonal matrix equation [17–19]. Although compact schemes have fewer grid points in the stencil, their implicit nature accounts for the contribution from large number of nodes present in the domain which provides a higher spectral resolution even on a coarser mesh [5, 14, 17–19, 24].

Researchers have also focused their attention on the development of new DRP schemes [14,21,25]. While designing a numerical scheme, one aims for preserving physical dispersion relation across a complete wavenumber range. However, various existing numerical schemes are capable of preserving physical dispersion relation only for a limited part of the complete wavenumber spectrum. The DRP nature of the various difference schemes is usually observed for the low wavenumber components while spurious dispersion is associated with high wavenumber components [13,14]. Spurious waves which are associated with the extreme form of a dispersion error in which computed scales not only travel with a wrong velocity but also in a wrong direction are identified as the q-waves [11, 13]. These spurious waves are often responsible for numerical instabilities [13,18,26]. Numerical instabilities can be avoided by either using numerical filters [18,20,26–29] or by using

https://doi.org/10.4208/cicp.101214.250515s Published online by Cambridge University Press

upwind scheme [17, 21, 30]. However, use of upwind schemes or multi-dimensional filters should not result into unphysical attenuation of the low wavenumber components. A new multi-dimensional adaptive filtering methodology was suggested in [28, 29] to attenuate high wavenumber components when and where it is absolutely necessary.

Researchers working in the area of Direct Numerical Simulation (DNS) and Large Eddy Simulation (LES) of complex turbulent flows suggested alternative techniques such as changing governing equations itself [31, 32] or the use of a staggered mesh [33, 34] to minimize spurious oscillations. In order to control the numerical instabilities associated with high wavenumber components, use of hyper-viscosity term in spectral methods [35–37] and the spectral vanishing viscosity method [38–40] has been suggested. In the particular context of the use of compact schemes in DNS/LES of turbulent flows, [41] suggested to introduce an extra-dissipation directly enclosed in the viscous term of the Navier-Stokes equations through a specific finite difference scheme for the computation of second derivatives. In the same work, an application for an aeroacoustic test case has also been provided.

In the present work, a new coupled compact difference scheme has been proposed to achieve significantly improved numerical properties. The full domain matrix global spectral analysis (GSA) technique [5, 12, 14, 17] is used to obtain the important numerical properties. It is shown that the numerical properties of the newly derived coupled compact difference scheme are superior as compared to the existing high accuracy schemes. Applicability of the proposed scheme has been shown by solving various acoustic and model wave propagation problems as well as by obtaining solution of the Navier-Stokes equation for the fluid flow problem. In the present work, a new methodology for the adaptive numerical diffusion is also presented. The merit of the present scheme in damping out unwanted reflected spurious disturbances from the domain boundaries is shown. Thus, the present scheme can also be used to provide an artificial absorbing layer to attenuate spurious reflections similar to the Perfectly Matched Layer (PML) technique.

Present manuscript has been arranged in the following way. In the next section, we discuss construction and numerical properties of the proposed coupled compact difference scheme. We have further applied the coupled compact difference scheme to simulate model wave equation problems as well as solution of Navier-Stokes equations in Section 3. Manuscript ends with important conclusions and summary in Section 4.

2 Construction and numerical properties of the coupled compact difference scheme

The solution of the Navier-Stokes equations needs evaluation of the first and the second order spatial derivative terms associated with flow convection and dissipation, respectively. High accuracy compact difference schemes were reported in [15–19, 21, 42] for the evaluation of the spatial derivative terms. Use of compact difference scheme requires special attention to suppress the numerical instabilities arising out of unphysical growth

https://doi.org/10.4208/cicp.101214.250515s Published online by Cambridge University Press

of the high wavenumber components. Numerical instabilities can be avoided by using upwind schemes in which an explicit numerical diffusion [14] term is added as expressed in the following equation:

$$\frac{\partial u}{\partial x}=\left(\frac{\partial u}{\partial x}\right)_{CD}+\alpha\left(\frac{\partial^{2n}u}{\partial x^{2n}}\right)h^{2n-1}, \tag{2.1}$$

where α is a diffusion coefficient, n is an integer and the subscript CD indicates derivative has been obtained using central difference scheme. The extra term $\alpha\left(\frac{\partial^{2n}u}{\partial x^{2n}}\right)h^{2n-1}$ in Eq. (2.1) adds numerical diffusion. The diffusion coefficient α can either be positive or negative based on the direction of propagation of information at a particular point and is used to control amount of added numerical diffusion. Note that the second derivative in the Navier-Stokes equations is associated with the physical dissipation process and usually a fourth or higher order even derivative terms are used for introducing numerical diffusion [14]. In this context, we developed a numerical scheme which evaluates the first, the second and the fourth derivative terms in a coupled manner.

A high accuracy spectrally optimized upwind scheme has been proposed in [21] which evaluates the first and the second derivative terms together. However, this scheme does not provide an option of adaptive numerical diffusion and attenuates the solution at each time step and at all grid points. Use of such schemes may result in unphysical attenuation of solution components. In the present work, we derive a new coupled compact difference scheme which has an advantage of adaptive numerical diffusion.

Consider a computational domain constructed using grid points with a uniform grid spacing h. Simultaneous evaluation of the first, the second and the fourth derivative terms using coupled compact difference scheme is expressed as

$$\begin{aligned}&a_1(u'_{i+1}+u'_{i-1})+u'_i+b_1h(u''_{i+1}-u''_{i-1})+c_1h^3(u''''_{i+1}-u''''_{i-1})\\&=\frac{1}{h}d_1(u_{i+1}-u_{i-1}),\end{aligned} \tag{2.2}$$

$$\begin{aligned}&\frac{a_2}{h}(u'_{i+1}-u'_{i-1})+b_2(u''_{i+1}+u''_{i-1})+u''_i+c_2h^2(u''''_{i+1}+u''''_{i-1})\\&=\frac{1}{h^2}(d_2(u_{i+1}+u_{i-1})+e_2u_i),\end{aligned} \tag{2.3}$$

$$\begin{aligned}&\frac{a_3}{h^3}(u'_{i+1}-u'_{i-1})+\frac{b_3}{h^2}(u''_{i+1}+u''_{i-1})+c_3(u''''_{i+1}+u''''_{i-1})+u''''_i\\&=\frac{1}{h^4}(d_3(u_{i+1}+u_{i-1})+e_3u_i).\end{aligned} \tag{2.4}$$

The various coefficients present in Eqs. (2.2)-(2.4) are found using Taylor series approxi-

https://doi.org/10.4208/cicp.101214.250515s Published online by Cambridge University Press

mations as tabulated below:

$$a_1=\frac{31}{64};\quad b_1=\frac{-5}{64};\quad c_1=\frac{1}{960};\quad d_1=\frac{63}{64},$$
$$a_2=\frac{313}{224};\quad b_2=\frac{-41}{224};\quad c_2=\frac{1}{672};\quad d_2=\frac{24}{7};\quad e_2=\frac{-48}{7},$$
$$a_3=\frac{-1725}{56};\quad b_3=\frac{285}{56};\quad c_3=\frac{-3}{56};\quad d_3=\frac{-360}{7};\quad e_3=\frac{720}{7}.$$

Eqs. (2.2)-(2.4) are solved in a coupled and iterative manner for the evaluation of the first, the second and the fourth derivative terms. As an initial guess, the various derivative terms are evaluated using explicit central difference schemes. Eqs. (2.2)-(2.4) are solved iteratively until the maximum residue falls below the prescribed tolerance value. Iterations can be performed by using either the traditional Gauss-Seidel iterative algorithm or a conjugate gradient method $(Bi-CGSTAB)$ [43].

For the non-periodic problems, we suggest the following stencils for the boundary and the near boundary nodes. Note that the second and the fourth derivative terms are not evaluated at the boundary nodes while the fourth derivative is not evaluated at the second and second last node

$$u_1'=(-1.5u_1+2u_2-0.5u_3)/h,\quad u_1''=0,\quad u_1''''=0, \tag{2.5}$$
$$u_2'=(u_3-u_1)/(2h),\quad u_2''=(u_1-2u_2+u_3)/h^2,\quad u_2''''=0, \tag{2.6}$$
$$u_3'=(-u_5+u_1+8(u_4-u_2))/(12h),\quad u_3''=(u_1-2u_2+u_3)/h^2,$$
$$u_3''''=(u_1+u_5-4(u_2+u_4)+6u_3)/h^4. \tag{2.7}$$

The stencils for the boundary and near boundary nodes on the other end of the domain can be similarly obtained [14].

Finite difference schemes are derived using Taylor series approximation in which one matches the required lower order derivative terms and truncates the higher order derivatives based on number of unknown coefficients. This results in difference between the numerically estimated and the exact derivative values. Thus, the use of difference scheme to evaluate a derivative of a function involves implicit filtering [14]. High accuracy schemes are designed specifically to obtain significant spectral resolution by minimizing implicit filtering involved in difference approximations [14, 17, 21]. Spectral resolution of a numerical scheme is a key design parameter for the construction of high accuracy scheme.

Consider a physical domain divided into N equi-spaced grid points with grid spacing h. The physical variable u_j at the j^{th} grid point can be represented in the spectral plane as [14], $u_j=\int U e^{iKx_j}\,dK$, where K is a wavenumber. Expression for the corresponding exact derivative is represented in the spectral plane as, $(u_j')_{exact}=\int iK U e^{iKx_j}\,dK$. However, when the same derivative has been evaluated numerically, truncation of the higher order derivative terms brings deviation in the numerically estimated derivative value as compared to the exact value. Thus, one can represent the numerically estimated derivative

https://doi.org/10.4208/cicp.101214.250515s Published online by Cambridge University Press

value in the spectral plane as [14], $(u'_j)_{numerical} = \int iK_{eq}\, U\, e^{iKx_j}\, dK$. The discretization effectiveness of a numerical scheme in evaluating the first derivative term can be given by variation of the ratio of K_{eq}/K across a complete wavenumber range. Ideally numerical scheme should have discretization effectiveness as one across a complete wavenumber range, however for various difference schemes this ratio starts deviating from the ideal value in high wavenumber range [14].

Here, we have followed the full domain matrix global spectral analysis (GSA) technique [5,12,14,17] to estimate spectral resolution of different difference schemes. The first derivative obtained using proposed coupled compact difference scheme is eighth order accurate based on Taylor series approximation. Two difference schemes can have same order of accuracy but different resolving abilities. This aspect has been shown by plotting spectral resolutions of eighth order accurate explicit and eighth order accurate implicit spatial difference schemes along with proposed coupled compact difference scheme in Fig. 1(a) while evaluating the first order derivative term. As the scheme with higher resolving ability produces more accurate result, proposed coupled compact difference scheme is useful for high accuracy computations in contrast to the traditional difference approximations having same order of accuracy.

In Fig. 1(a), we have also shown the spectral resolutions for the *CCD* scheme of [42] which has a central stencil and the spectrally optimized upwind *CCD* scheme of [21] in evaluating the first derivative term. We have purposefully compared numerical properties of proposed scheme with *CCD* schemes of [21] and [42] as these schemes also evaluate the first and the second derivative terms using the information available at the next and previous grid points only. Fig. 1(a) shows the discretization effectiveness of the coupled compact difference scheme lies in between that of *CCD* scheme of [21] and [42].

Although spectrally optimized *CCD* scheme of [21] displays higher resolving ability than the present scheme, it has a disadvantage of implicit addition of numerical diffusion to the solution as evident from the variation of the imaginary part of K_{eq}/K as shown in the Fig. 1(b). Thus, the upwind *CCD* scheme in [21] numerically attenuates the resolved high wavenumber components at each grid point and at each time step. Ideally, one should add numerical diffusion whenever it is absolutely required to avoid numerical instabilities.

For the derived numerical scheme, estimation of the discretization effectiveness for the second order derivative terms $(-K_{eq}^2/K^2)$ associated with viscous dissipation process in the Navier-Stokes equation, is also important. Fig. 1(c) compares the spectral resolutions for the indicated difference schemes in estimating second derivative. All the schemes have a near spectral resolution. One observes a mild overshoot of the discretization effectiveness above ideal value one near the Nyquist limit. Authors in [30] concluded that over prediction of the spectral amplitude for the second derivative in the high wavenumber region helps in de-aliasing the numerical solution.

In addition to the estimation of the second order derivative terms, computation of higher order even derivative term is essential to obtain numerical stability through addition of numerical diffusion as shown in Eq. (2.1). In the present work, we evaluate

https://doi.org/10.4208/cicp.101214.250515s Published online by Cambridge University Press

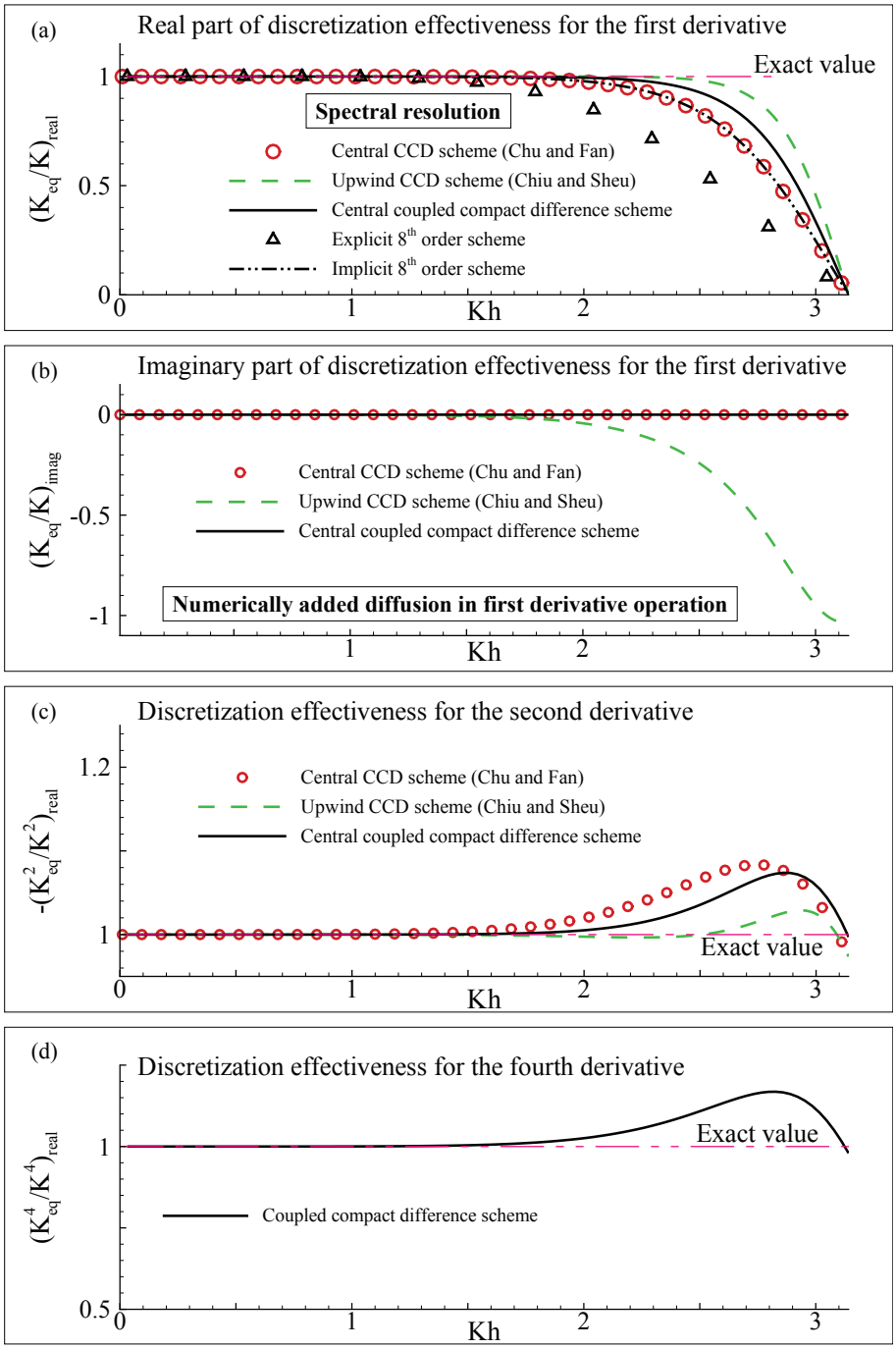


Figure 1: Comparison of the discretization effectiveness in evaluating the first, the second and the fourth derivative terms for the indicated spatial discretization schemes at the central node has been shown. Here, K and K_{eq} denote the exact and the numerically obtained wavenumber, respectively.

https://doi.org/10.4208/cicp.101214.250515s Published online by Cambridge University Press

a fourth order derivative term for adding numerical diffusion. Fig. 1(d) shows the discretization effectiveness for evaluating the fourth derivative term (K_{eq}^4/K^4) using coupled compact difference scheme. Similar to the effectiveness variation of the second derivative term, effectiveness of fourth derivative term is overestimated in the high wavenumber range which provides more control on aliasing error as discussed in [30]. Numerical instabilities are usually observed due to amplification of high wavenumber components [13, 14, 18]. Thus, addition of numerical diffusion is aimed at attenuating high wavenumber components.

Prior to simulating complex unsteady problems, one needs to analyze other important numerical properties such as the numerical amplification factor $|G|$ and the normalized numerical group velocity V_{gN}/c for the solution of model one dimensional $(1D)$ wave equation [12, 14] given by

$$\frac{\partial u}{\partial t}+c\frac{\partial u}{\partial x}=0, \quad c>0. \tag{2.8}$$

Eq. (2.8) has a non-dispersive and non-dissipative nature. Analytical solution of Eq. (2.8) suggests that the initial disturbance will travel with a constant phase velocity c without attenuation or amplification of signal amplitude. Since the acoustic waves are non-dispersive and there is no appreciable change in their amplitude over a small distance [6], Eq. (2.8) becomes a model equation for justifying applicability of numerical schemes in simulating acoustic signal propagation. Thus in the present work, we obtain the $|G|$ and the V_{gN}/c contours for the solution of 1D wave equation following the work in [12, 14]. Numerical amplification factor for the j^{th} node G_j is defined as the ratio of the spectral amplitudes of the signal at two successive instants $\left(G_j=\frac{U(K,t^{n+1})}{U(K,t^n)}\right)$ [12, 14]. In general, G_j is a complex number $(G_j=G_R+iG_I)$ and $|G_j|=\sqrt{(G_R^2+G_I^2)}$ [12, 14]. If one defines the phase angle β as $\tan\beta=-G_I/G_R$ then one can write the expressions for the normalized numerical group velocity V_{gN}/c and normalized numerical phase speed c_N/c following the work in [12, 14] as

$$\left[\frac{c_N}{c}\right]_j=\frac{\beta_j}{\omega\Delta t}, \tag{2.9}$$

$$\left[\frac{V_{gN}}{c}\right]_j=\frac{1}{N_c}\frac{d\beta_j}{d(Kh)}, \tag{2.10}$$

where N_c is a non-dimensional CFL number, h is a uniform grid spacing and Δt is an incremental time step. A detailed description on the evaluation of $|G_j|$, V_{gN}/c and c_N/c properties is presented in [14] and skipped here to avoid repetition.

Fig. 2 compares the $|G|$ and V_{gN}/c properties for the central node when the indicated spatial discretization schemes and the $RK4$ time integration scheme are used for the solution of the 1D wave equation (2.8). The left and the right frames of the Fig. 2(a) show $|G_j|$

https://doi.org/10.4208/cicp.101214.250515s Published online by Cambridge University Press

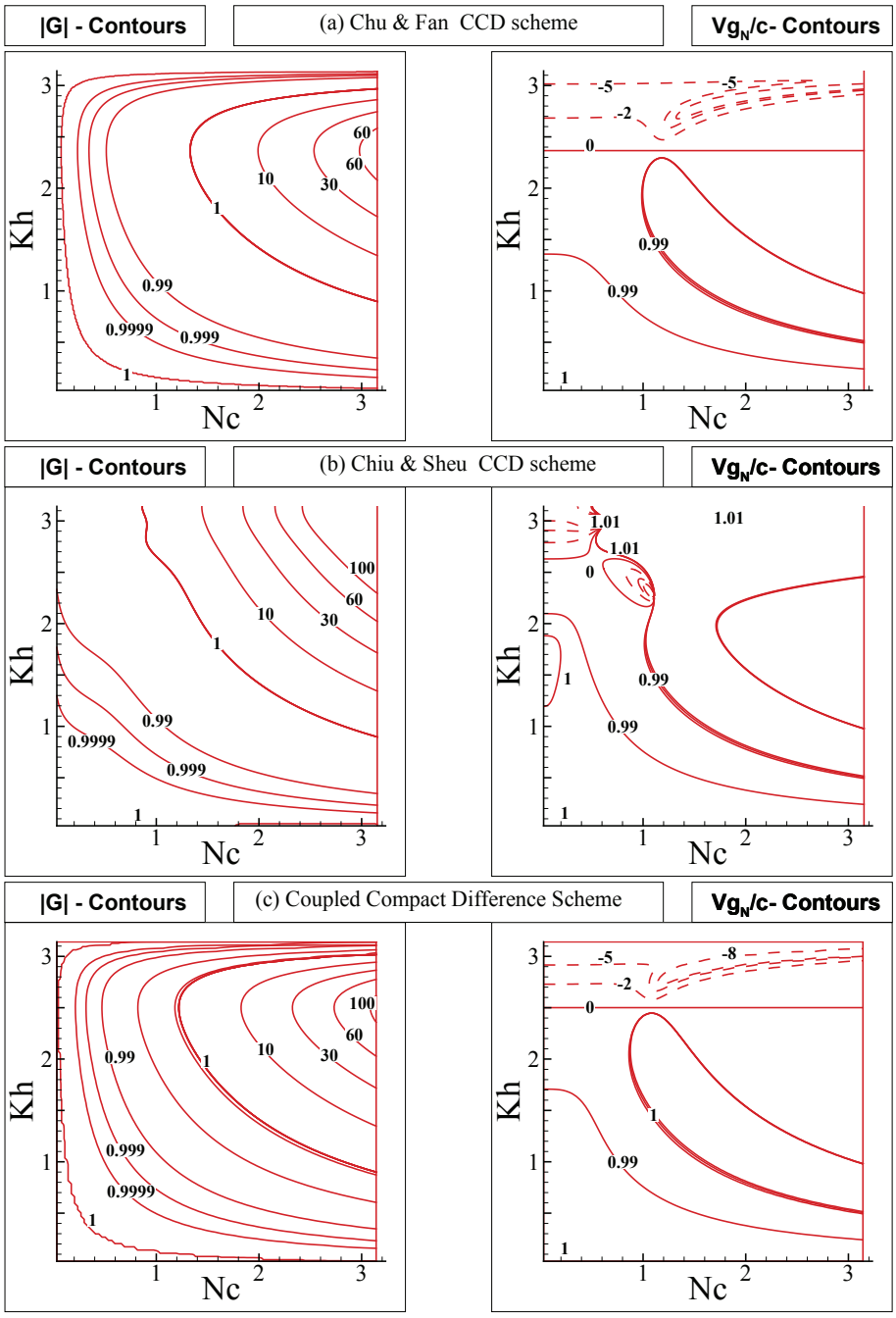


Figure 2: Variations of the numerical amplification factor $|G|$ and normalized group velocity V_{gN}/c contours for the central node are shown when the spatial discretization is performed using (a) CCD scheme of [42]; (b) CCD scheme of [21] and (c) coupled compact difference scheme along with $RK4$ time integration scheme for the solution of the 1D wave equation.

https://doi.org/10.4208/cicp.101214.250515s Published online by Cambridge University Press

and V_{gN}/c contours as a function of the CFL number N_c and non-dimensional wavenumber Kh when no numerical diffusion ($\alpha=0$) has been explicitly added to the spatial discretization term. The $|G_j|$ contours in Fig. 2(a) and (c) show the desired neutrally stable region ($|G|=1$) for a small value of N_c across a complete band of Kh. Solution components in this region will be neither amplified nor attenuated numerically as desired for the solution of computational acoustic problems. However, such neutrally stable region is absent for CCD scheme of [21] ($|G|<1$) due to the upwind nature of the scheme.

The region bound by $V_{gN}/c=0.99$ and $V_{gN}/c=1.01$ contour lines is identified as the DRP region [5, 12, 14, 25]. The V_{gN}/c contours show that for a CFL number less than $N_c=0.15$ one obtains DRP region up to $Kh=1.70$. Solution components above this wavenumber value will be spurious as they propagate with different speed compared to physical propagation speed. All the indicated spatial discretization schemes in Fig. 2 show extreme form of dispersion error, also called as q-waves [12–14] in the high Kh range.

For a correct prediction of the acoustic field, any spurious components presented in the solution must be strongly attenuated. In this regard, we propose addition of controlled amount of numerical diffusion through the evaluated fourth derivative term whenever and wherever it is required. Here, numerical diffusion has been added as shown in Eq. (2.11) where the first and the fourth derivatives are obtained by solving Eqs. (2.2)-(2.4)

$$\frac{\partial u}{\partial x}=\frac{\partial u}{\partial x}+\alpha\left(\frac{\partial^4 u}{\partial x^4}\right)h^3. \tag{2.11}$$

For the proposed scheme, effects of the added numerical diffusion on the $|G|$ and V_{gN}/c properties are shown in Fig. 3. Top row frames show the numerical properties corresponding to diffusion coefficient $\alpha=0.001$. Due to addition of explicit numerical diffusion following Eq. (2.11), loss of neutrally stable region is observed in Fig. 3 for a small CFL number values across complete wavenumber range. Addition of numerical diffusion results in stability at the small CFL number range as displayed by the $|G|<1$ contours. Numerical amplification $|G|$ contours in Fig. 3(a)-(c) show that as the diffusion coefficient increases from a moderate value of $\alpha=0.001$ to $\alpha=0.01$, scheme becomes more stable. Quantitative information provided by these contours helps to choose appropriate value of diffusion coefficient α for the simulations. In Fig. 3, one observes $|G|$ values are close to one for small CFL values in the low wavenumber range. However, the spurious high wavenumber components are severely attenuated due to smaller $|G|$ values. Thus, addition of numerical diffusion helps to attenuate spurious unphysical high wavenumber components. The group velocity contours in Fig. 3 show another interesting behavior. As one adds more numerical diffusion, the q-wave region shrinks in size and solution becomes less susceptible to numerical instabilities arising from q-waves.

Fig. 4 shows numerical amplification factor properties for inlet boundary and the near boundary nodes in the absence of explicit numerical diffusion. For non-periodic problems one needs to use different boundary stencils at the boundary and near boundary

https://doi.org/10.4208/cicp.101214.250515s Published online by Cambridge University Press

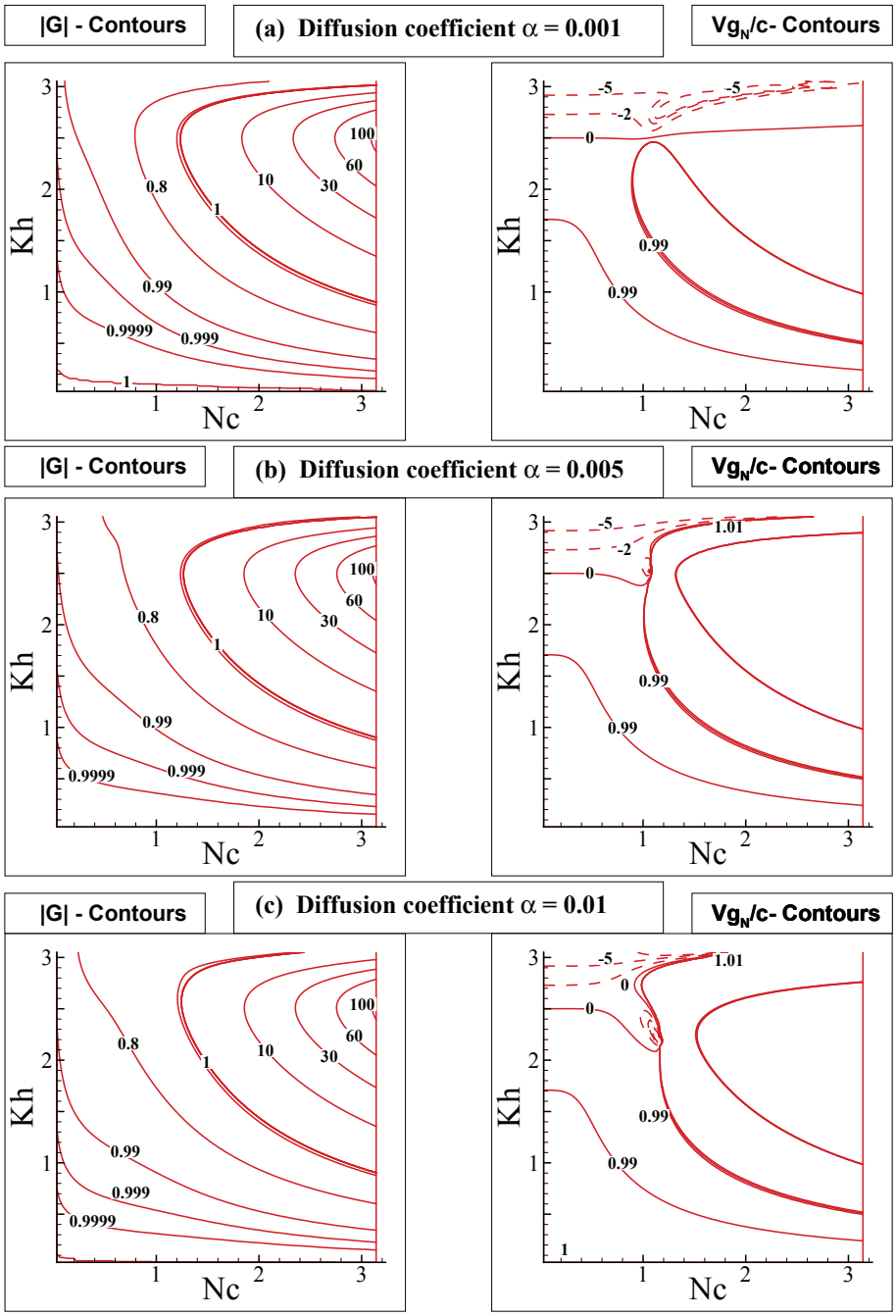


Figure 3: Effects of diffusion coefficients on the variations of the numerical amplification factor $|G|$ and normalized group velocity V_{gN}/c contours for the central node are shown when the spatial discretization is performed using coupled compact difference scheme along with $RK4$ time integration scheme for the solution of the 1D wave equation.

https://doi.org/10.4208/cicp.101214.250515s Published online by Cambridge University Press

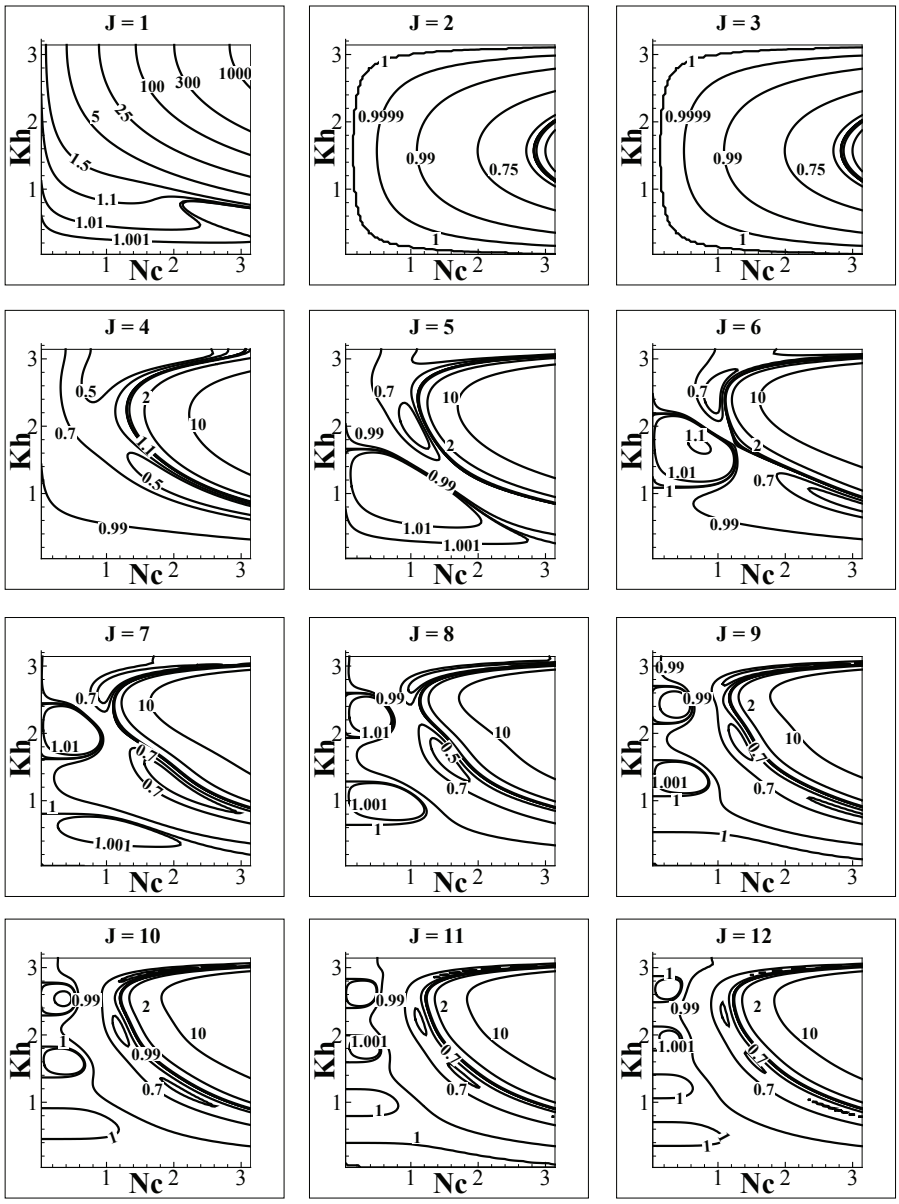


Figure 4: Comparison of the numerical amplification factor $|G|$ contours for the boundary and near boundary nodes when the coupled compact difference scheme is used with $RK4$ time integration scheme for 1D wave equation. Domain has been divided into 101 equi-spaced grid points with h as a uniform grid spacing.

nodes. This results in different numerical properties for the near boundary nodes as compared to the nodes located in the interior region [14]. The $|G_j|$ contours for the node $J=1$ show massive unstable region even for small CFL values. As we have used central explicit stencils for nodes 2 and 3, these nodes show necessary neutrally stable region for

https://doi.org/10.4208/cicp.101214.250515s Published online by Cambridge University Press

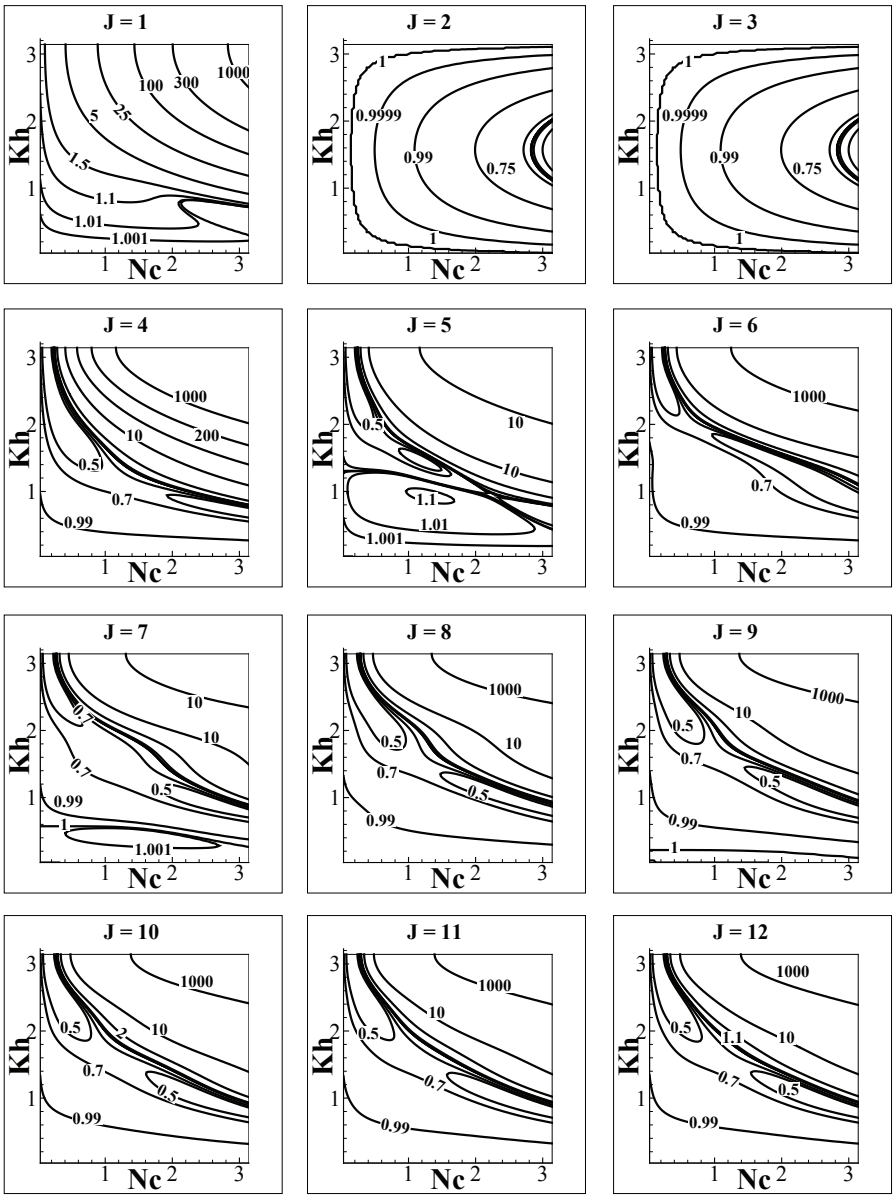


Figure 5: Comparison of the effects of addition of numerical diffusion parameter $\alpha = 0.01$ on the variation of the numerical amplification factor $|G|$ contours for the boundary and near boundary nodes when the coupled compact difference scheme is used with $RK4$ time integration scheme for 1D wave equation. Domain has been divided into 101 equi-spaced grid points with h as a uniform grid spacing.

small CFL values. However, from node 5 onwards one observes mild unstable nature for small CFL values.

Unstable nature of near boundary nodes can be eliminated by adding numerical diffusion. Fig. 5 shows variation of $|G_j|$ contours for the boundary and near boundary nodes

https://doi.org/10.4208/cicp.101214.250515s Published online by Cambridge University Press

when the fourth order diffusion term with diffusion coefficient $\alpha = 0.01$ is added to the first derivative. Figure shows that with the addition of numerical diffusion, $|G_j|$ contours show stable nature for small CFL values. Thus, one can carefully choose appropriate value of diffusion coefficient and achieve desired numerical properties. Note that numerical instabilities are often triggered when spurious q-waves reach unstable inlet nodes. If one eliminates spurious waves in the interior of the domain then there is no need to add numerical diffusion for near boundary nodes. Figs. 4 and 5 highlight inferior properties of the near boundary nodes as compared to the central node shown in Fig. 2(c).

3 Results and discussion

In this section, the coupled compact difference scheme has been applied to solve the various model wave equation problems as well as 2D Navier-Stokes equations to test the efficacy. Various test cases discussed in this work display development of complex acoustic/flow field. Solutions for the problems of 1D wave equation and the spherical wave propagation are obtained to check the dispersive and dissipative nature of the present scheme. In these examples, methodology for adaptive numerical diffusion has been developed. A model computational acoustic problem related to the development of an acoustic field due to the acoustic radiations originated from an oscillating circular piston has also been solved. Use of the derived coupled compact difference scheme as an alternative approach to the PML technique has been shown by solving 2D Navier-Stokes equations for the case of a convecting vortex.

3.1 Solution of 1D wave equation

Here, we have solved 1D wave equation as given by Eq. (2.8) and demonstrated ability of the coupled compact difference scheme to correctly resolve the steep gradients present in the solution. We have considered a domain $0 \leq x \leq 200$ with 1001 equi-spaced grid points. Computations are performed using the coupled compact difference scheme for the spatial discretization and $RK4$ scheme for the time integration by keeping CFL number as 0.01. Phase speed c is kept as unity. For the present problem, the initial condition has been prescribed as

$$u(x,0) = e^{-0.20(x-80)^2} + 0.1 \times e^{-1.60(x-50)^2}. \tag{3.1}$$

The initial condition is specifically designed as a superposition of a smooth wave packet of unit amplitude located at $x = 80$ and a wave packet with sharp gradient located at $x = 50$. Traditional explicit low resolution schemes can resolve the smooth low wavenumber packet accurately. However, these schemes can not resolve a large bandwidth of wavenumber generated at the sharp gradients or discontinuities. Insufficient resolution creates spurious waves which in turn provide seed for numerical instability.

Initial condition in Eq. (3.1) has been shown in Fig. 6(a). Numerical solution at $t = 20$ is displayed in Fig. 6(b). Vertical dashed lines at $x = 70$ and $x = 100$ denote the exact

https://doi.org/10.4208/cicp.101214.250515s Published online by Cambridge University Press

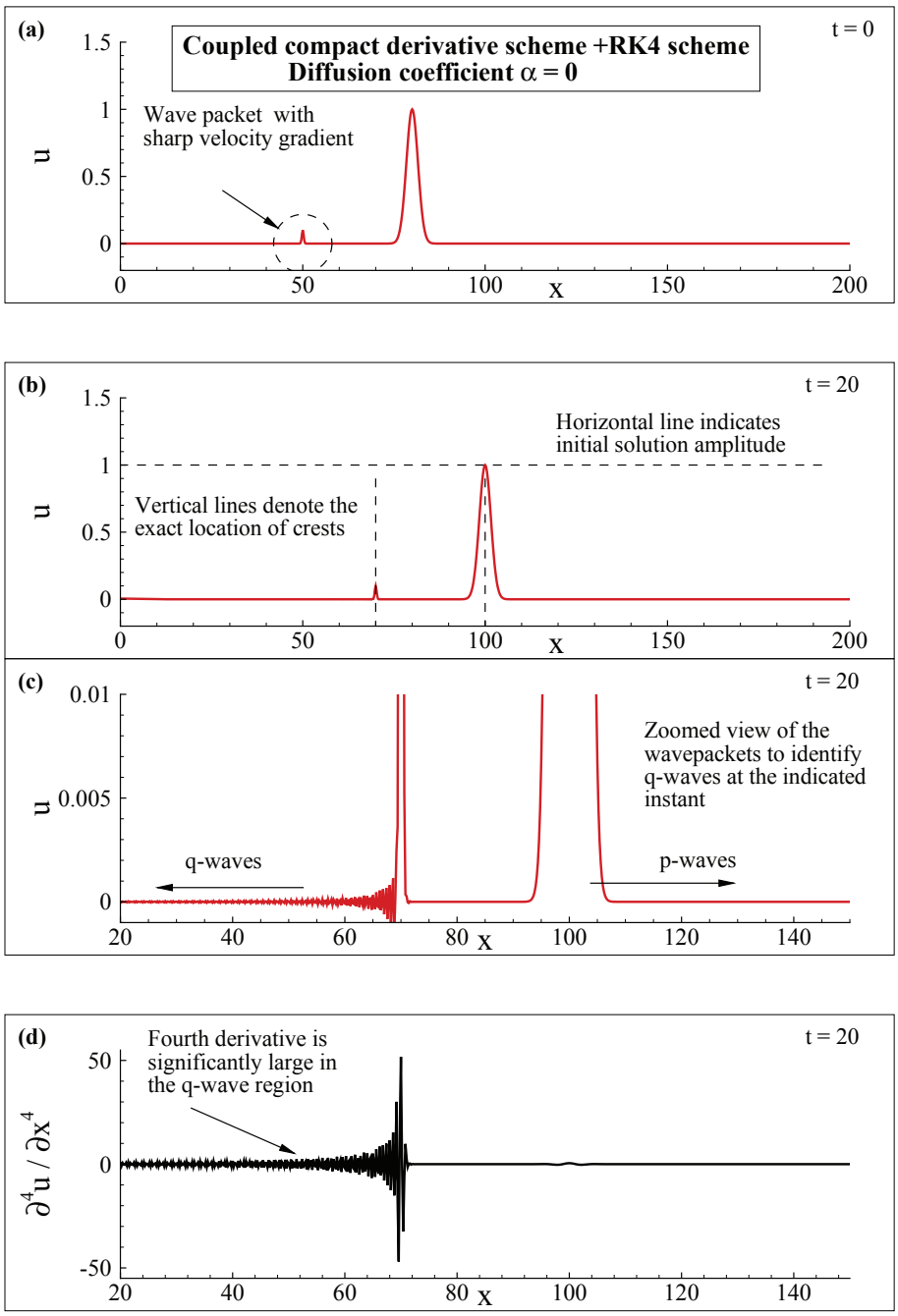


Figure 6: Solution of the 1D wave Eq. (2.8) using proposed coupled compact difference scheme and $RK4$ time integration scheme without addition of numerical diffusion; (a) Initial condition; (b) Solution at $t=20$; (c) Zoomed view of the solution in (b) close to line $u=0$ is shown to mark spurious waves; (d) Fourth derivative of solution amplitude is significant in the q-wave region as these waves are associated with high wavenumber components.

https://doi.org/10.4208/cicp.101214.250515s Published online by Cambridge University Press

locations of crest for the sharp and the smooth wave packets, respectively. Horizontal dashed line at $u=1.0$ denotes the initial amplitude of the smooth packet and is drawn for comparison. Fig. 6(b) shows that the smooth as well as the sharp gradient packets are well captured by the coupled compact difference scheme. Due to the significant spectral resolution and the DRP nature of the coupled compact difference scheme, no significant dispersion is noted. However, only if one zooms the region close to $u=0$ line as shown in Fig. 6(c) then the spurious q-waves are observed. Although the q-waves have small amplitude, these are capable of triggering numerical instabilities [13, 18].

One can use the information available with the evaluated fourth derivative term in the coupled compact difference scheme to locate q-waves as shown in Fig. 6(d). Differentiation operation magnifies the solution discontinuities [29]. The spurious q-waves are primarily associated with the high wavenumber components. Evaluation of the higher order derivative term magnifies the discontinuities present in the solution. Fig. 6(d) shows that the fourth derivative corresponding to the low wavenumber packet is negligible while it shoots up in the region of q-waves.

In the present work, we have suggested a new methodology for introducing adaptive numerical diffusion based on solution gradients. Addition of the numerical diffusion is based on the amplitude of the fourth derivative of solution variable. One can prescribe a limiting amplitude for q-waves above which spurious waves will be attenuated by adding numerical diffusion. Thus in the adaptive numerical diffusion methodology, numerical diffusion is added only if the fourth derivative of the solution is above certain limiting value which indicates presence of significant high wavenumber components. Fig. 6(d) shows without addition of numerical diffusion, amplitude of the fourth derivative associated with the spurious wave region lie between ± 50. In Fig. 7(b) we have obtained the numerical result by adding numerical diffusion with diffusion coefficient $\alpha=0.01$ only for the region where the amplitude of the fourth derivative is greater than ± 1. If the value of a fourth derivative at a particular grid point is more than 2% of the total dynamic range of fourth derivative in the domain, then we have added numerical diffusion. The criterion for addition of numerical diffusion should be such that it should remove undesirable q-waves from the solution without causing unphysical attenuation of solution components. Thus, depending on the nature of the problem and used grid, adaptive diffusion criterion is subjected to change. Addition of the numerical diffusion significantly attenuates spurious q-waves as observed in the zoomed view of Fig. 7(c) and the variation of the fourth derivative of solution amplitude in Fig. 7(d). However, due to the adaptive nature associated with the numerical diffusion, low wavenumber components remain unattenuated as shown in Fig. 7(b). This is an important advantage of the adaptive diffusion ability of the newly derived coupled compact difference scheme.

In order to compare effectiveness of proposed scheme as compared to the available high accuracy schemes, we have once again solved the same 1D wave equation problem by using spectrally optimized upwind *CCD* scheme of [21]. Figs. 8(a) and 8(b) again show the same initial condition given by Eq. (3.1) and the computed solution at $t=20$, respectively. Due to the addition of the numerical diffusion, spurious waves are com-

https://doi.org/10.4208/cicp.101214.250515s Published online by Cambridge University Press

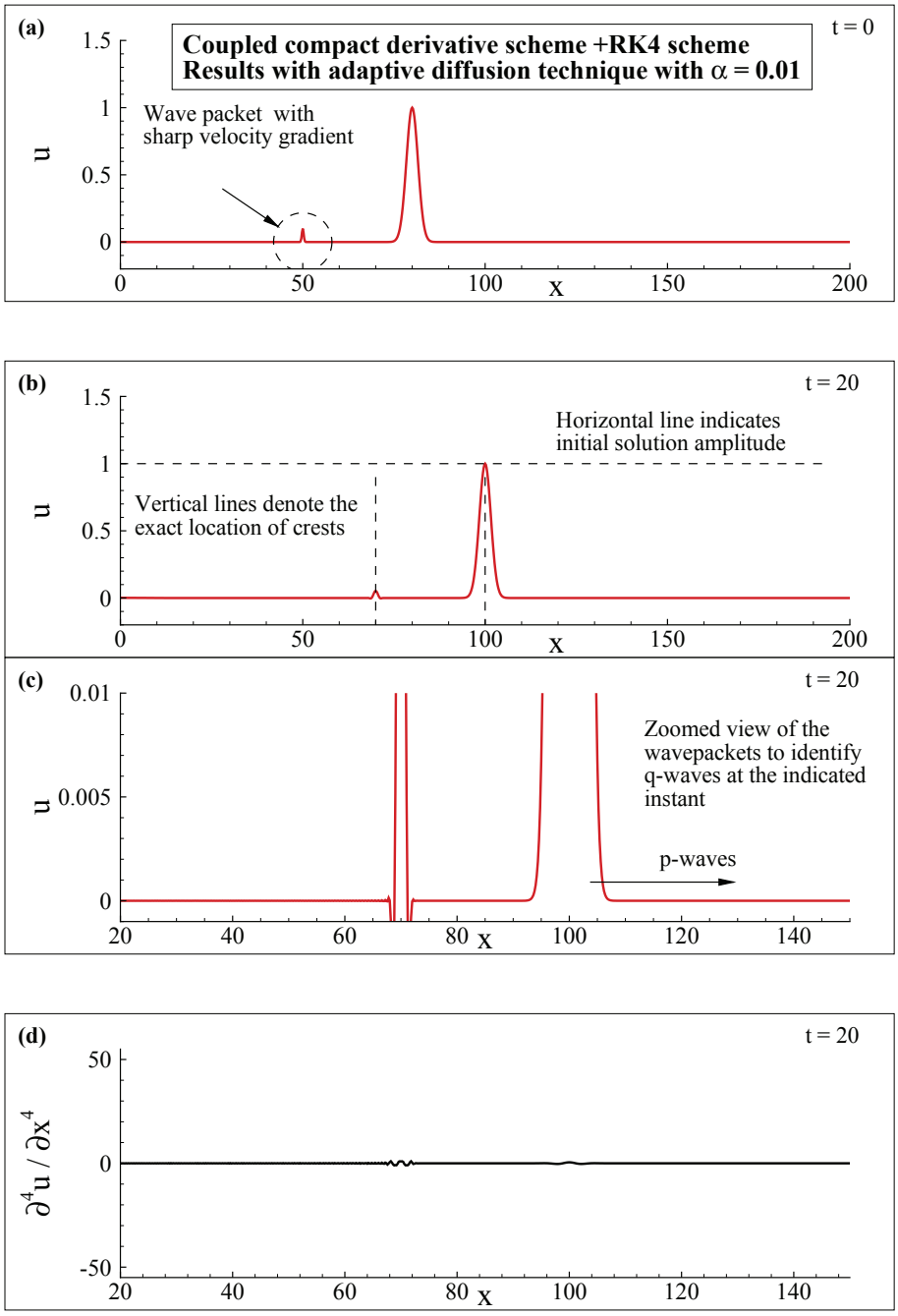


Figure 7: Solution of the 1D wave Eq. (2.8) using proposed coupled compact difference scheme and $RK4$ time integration scheme with adaptive addition of numerical diffusion following Eq. (2.11) with $\alpha=0.01$; (a) Initial condition; (b) Solution at $t=20$; (c) Zoomed view of the solution in (b) close to line $u=0$; (d) Fourth derivative of solution amplitude is insignificant due to attenuation of q-waves.

https://doi.org/10.4208/cicp.101214.250515s Published online by Cambridge University Press

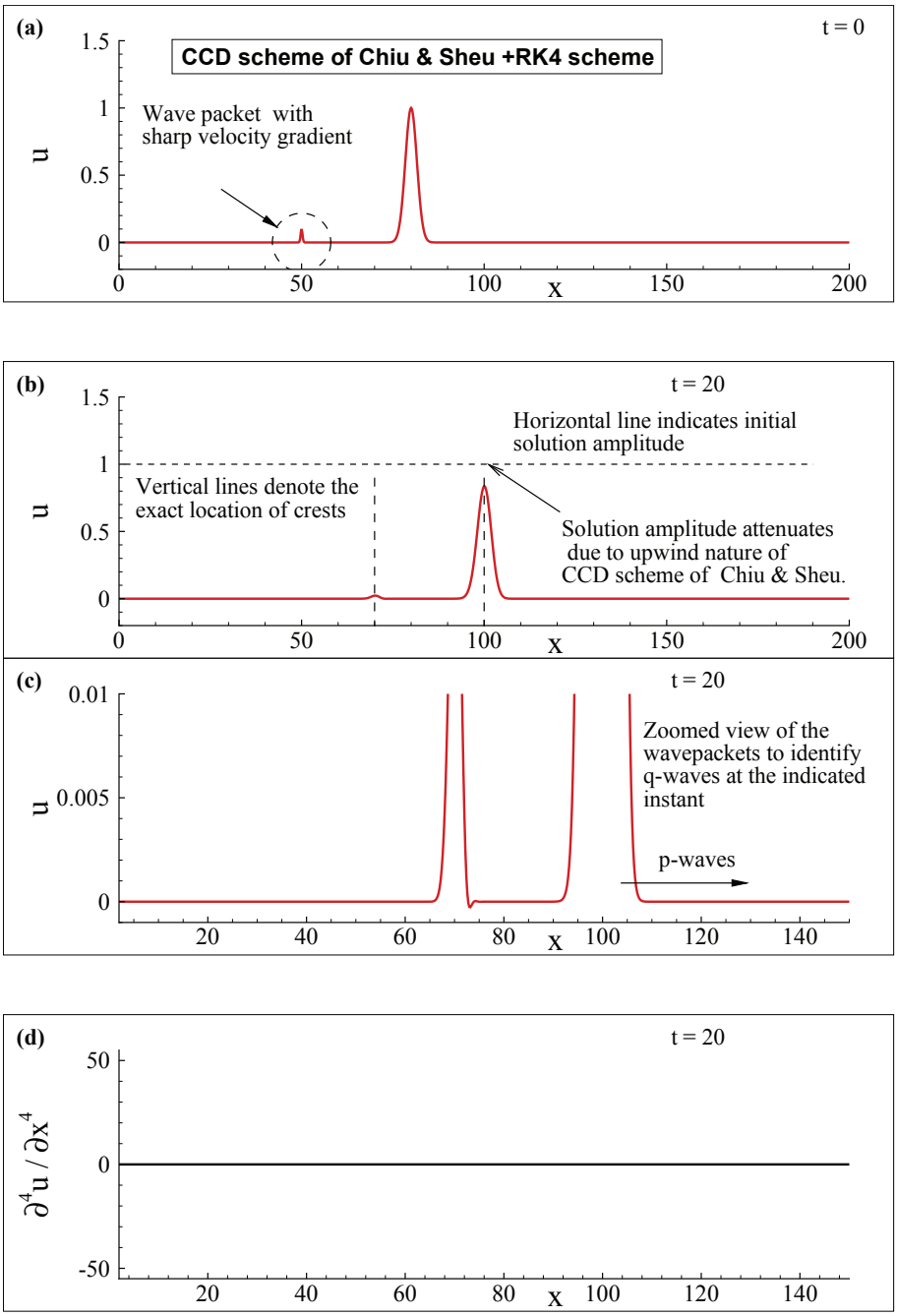


Figure 8: Solution of the 1D wave Eq. (2.8) using upwind CCD scheme of [21] and $RK4$ time integration scheme; (a) Initial condition; (b) Solution at $t=20$; (c) Zoomed view of the solution in (b) close to line $u=0$ is shown; (d) Fourth derivative of solution amplitude is insignificant due to attenuation of q-waves. Note the attenuation of low wavenumber (smooth) packet due to the implicit addition of numerical diffusion through upwind CCD scheme of [21].

https://doi.org/10.4208/cicp.101214.250515s Published online by Cambridge University Press

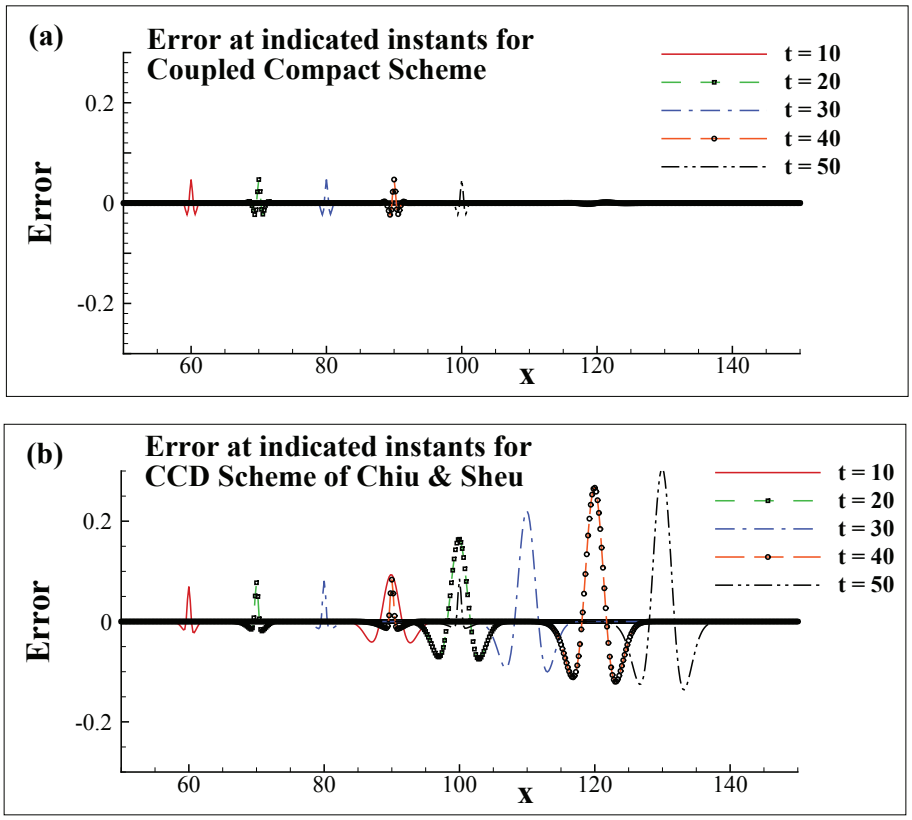


Figure 9: Comparison of the error in solving Eq. (2.8) by (a) coupled compact difference scheme and $RK4$ scheme and (b) CCD scheme in [21] and $RK4$ scheme. Note that although CCD scheme of [21] has higher spectral resolution and better DRP ability as compared to the coupled compact difference scheme, it's results display higher numerical error due to diffusive nature of the scheme.

pletely damped out as shown in the zoomed view in Fig. 8(c) and the fourth derivative of the solution amplitude in Fig. 8(d). However, upwind nature of the scheme causes loss of neutrally stable region as shown in the Fig. 2(b) and the smooth as well as the sharp gradient packets are severely attenuated as shown in Fig. 8(b). Thus, use of upwind schemes needs a careful attention.

Benefit of proposed scheme as compared to the high resolution scheme of [21] has been shown in Fig. 9 which shows comparison of the error in solving Eq. (2.8) when $RK4$ scheme has been used for time integration. The numerical error has been computed as the difference between the exact and the corresponding numerical solution at the given instant. Fig. 9 shows that error for the CCD scheme of [21] is one order more as compared to that of proposed scheme. Thus proposed scheme performs better on the similar stencil. Note that although CCD scheme of [21] has higher spectral resolution and better DRP ability as compared to the coupled compact difference scheme, it displays higher numerical error due to dissipative nature of the scheme.

https://doi.org/10.4208/cicp.101214.250515s Published online by Cambridge University Press

3.2 Solution of the spherical wave equation

Consider a propagation of a spherical wave, set up due to the prescribed monochromatic excitation in a physical domain $5\leq r\leq 450$ at the location $r=5$. Monochromatic excitation is given as $u=\sin\omega t$, where ω is a circular frequency. Propagation of the spherical wave governed by the spherical wave equation is given as [4]

$$\frac{\partial u}{\partial t}+\frac{u}{r}+\frac{\partial u}{\partial r}=0. \tag{3.2}$$

The computational domain has been divided into 891 equi-spaced grid points. Numerical solutions obtained for the present problem have been compared with the exact solutions for two different monochromatic excitations. The coupled compact difference scheme has been used for the spatial discretization while $RK4$ scheme has been used for the time integration. A time step is chosen corresponding to the CFL number $N_c=0.01$.

Figs. 10(a) and 10(b) show the propagation of the spherical wave following Eq. (3.2) at the indicated instants for two different excitations of $\omega=\pi/4$ and $\pi/3$, respectively. Amplitude of the wave is maximum at $r=5$ and it decreases progressively as wave propagates outward. The exact solution for the Eq. (3.2) is given in [4] as

$$u(r,t)=\frac{5}{r}\sin\Big[\omega(t-(r-5))\Big]. \tag{3.3}$$

Comparison of the exact and the obtained numerical solutions in Figs. 10(a) and 10(b) shows an excellent match. Thus, for the chosen excitation frequencies use of coupled compact difference scheme does not display dispersive and dissipative solution.

3.3 Acoustic radiations from an oscillating circular piston

Here, an acoustic field set up due to oscillating circular piston has been simulated. A 2D computational domain with $0\leq x\leq 400$, $-200\leq r\leq 200$ has been considered as shown in the schematic Fig. 11(a). The domain has been divided into 400 equi-spaced grid points in the x and r-directions. The wall and the piston are located at the line $x=0$. The governing equations of this model problem can be written in the cylindrical coordinates (r,x,θ) as [3]

$$\frac{\partial u}{\partial t}+\frac{\partial p}{\partial x}=0, \tag{3.4}$$

$$\frac{\partial v}{\partial t}+\frac{\partial p}{\partial r}=0, \tag{3.5}$$

$$\frac{\partial p}{\partial t}+\frac{\partial v}{\partial r}+\frac{v}{r}+\frac{\partial u}{\partial x}=0. \tag{3.6}$$

Although the present problem has been solved with an axi-symmetric approximation in [3] by considering a domain above the centerline of the piston $r=0$, here the lower

https://doi.org/10.4208/cicp.101214.250515s Published online by Cambridge University Press

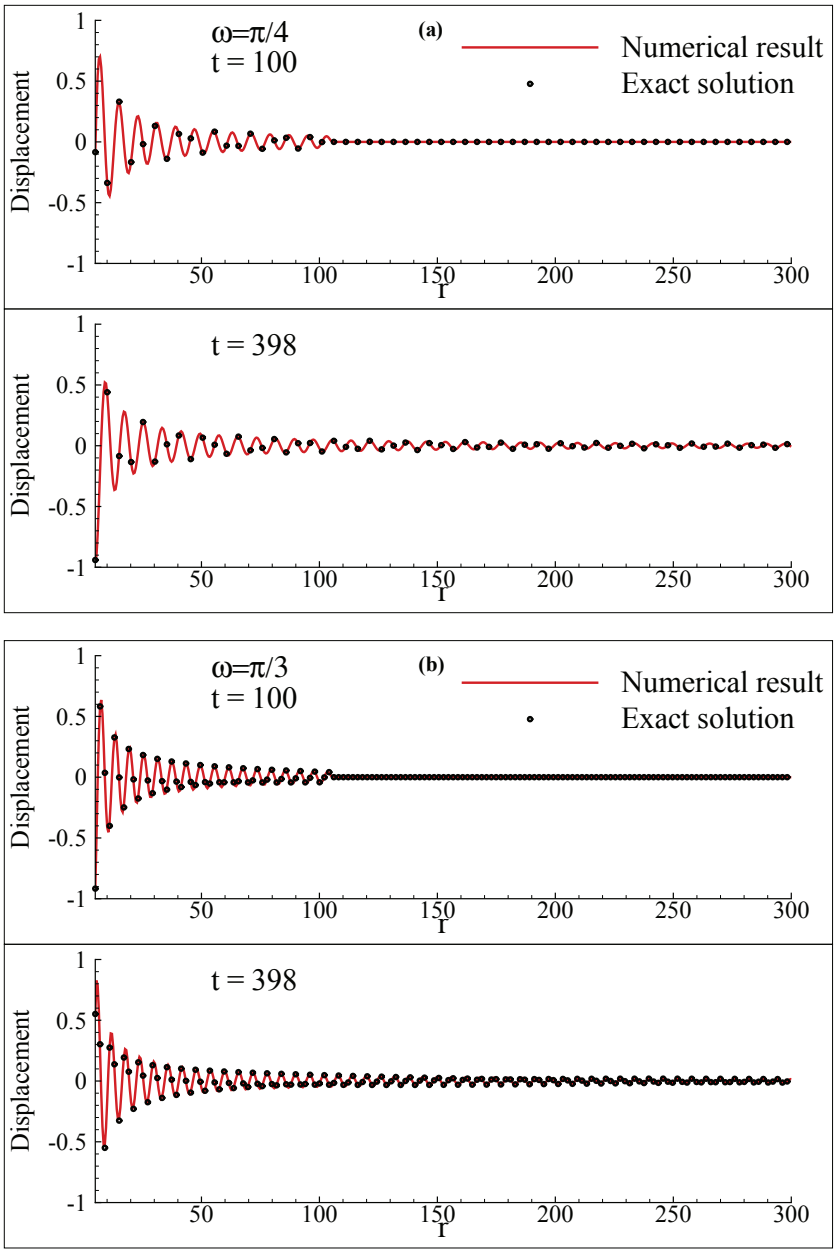


Figure 10: Wave propagation following spherical wave Eq. (3.2) is shown at the indicated instants and excitation frequencies in (a) and (b).

as well as upper parts of the domain have been considered. Eqs. (3.4) to (3.6) are solved in a coupled manner by using the coupled compact difference scheme for the spatial discretization while $RK4$ scheme has been used for time integration. Computations are performed with a time step of $\Delta t = 0.10$. Radius of the piston R is prescribed as 10. The

https://doi.org/10.4208/cicp.101214.250515s Published online by Cambridge University Press

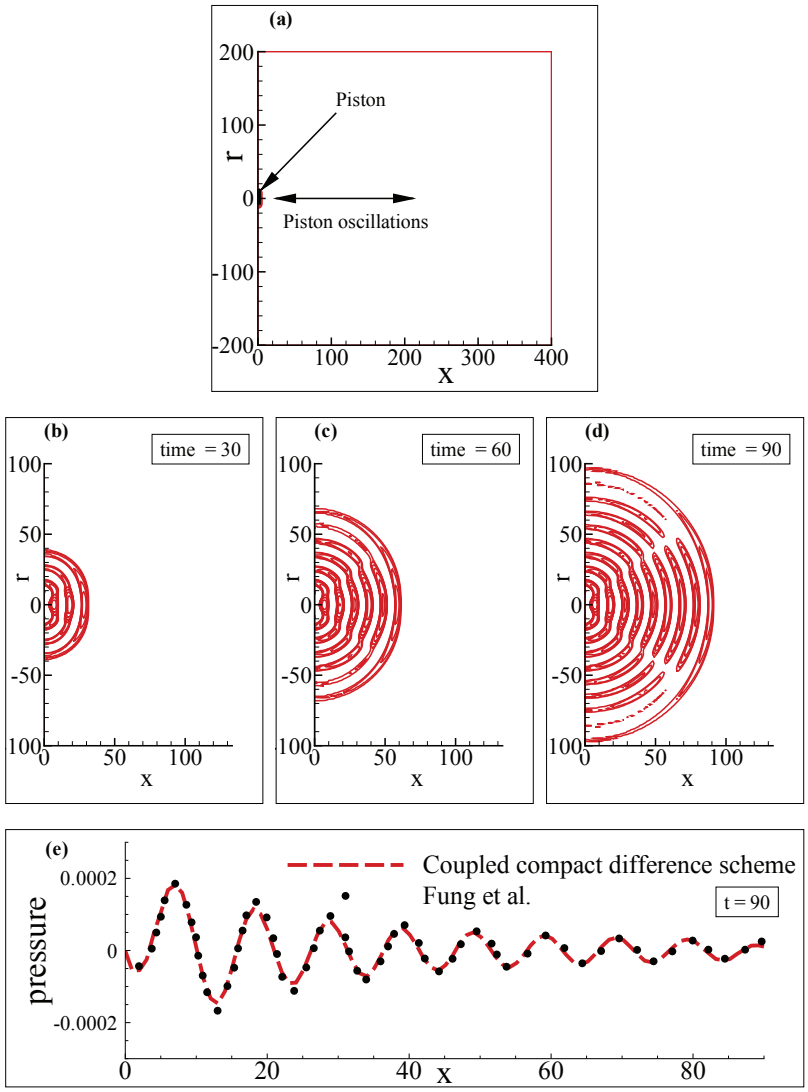


Figure 11: Schematic of the computational domain is shown in (a). Note the center of the oscillating piston is located at the origin and it oscillates along the line $r=0$. Instantaneous pressure contours set up due to piston oscillations are shown in (b), (c) and (d), respectively at the indicated times. Comparison of pressure variation on the line $r=0$ obtained from the present calculations to that of results in [3] is shown in (e).

boundary conditions on the wall surface $x=0$ are given as [3]

$$u=0, \quad |r|>10,$$
$$u=0.0001\sin\left(\frac{\pi t}{5}\right), \quad |r|\leq 10.$$

Pressure fluctuations radiating due to the monochromatic oscillations of the piston, set up an acoustic field in the domain. Development of the acoustic field with time has

https://doi.org/10.4208/cicp.101214.250515s Published online by Cambridge University Press

been shown in Figs. 11(b)-(d) at the indicated instants by plotting pressure contours. Figures show that with time acoustic disturbances travel radially outwards. Symmetry of acoustic field about the axis $r=0$ has been observed. Computed pressure fluctuations on the piston centerline $r=0$ are compared with the numerical results in [3] at the indicted instant and show a good agreement between the two. Thus the coupled compact difference scheme is useful for solving the computational acoustic problems.

3.4 Coupled Compact difference scheme as an alternative to the PML technique

While obtaining solution of 1D wave equation, merit of the coupled compact difference scheme for adaptive numerical diffusion has been demonstrated. In the next example, we show that the coupled compact difference scheme has been further utilized as the PML technique to absorb spurious reflections from the domain outflow boundary. In this example a discrete shielded vortex convecting in a uniform flow is studied. In order to solve Navier-Stokes equations, we have used the proposed coupled compact difference scheme for evaluating the first and the second order derivative terms while $RK4$ scheme is used for temporal integration. A computational domain of size $-1\leq(x,y)\leq 1$ is divided into 101 equi-spaced points in the respective directions. Flow enters the square domain $ABCD$ from the left boundary AD with a uniform velocity. At the center of the computational domain, a discrete shielded vortex [44] has been prescribed as an initial condition. Schematic of the chosen problem is as shown in Fig. 12(a). If we denote the distance between any point in the domain and the center of the vortex by symbol r then the discrete shielded vortex can be prescribed as in [44]

$$\omega = k\,(1-100\,r^2)\,e^{-100r^2}. \tag{3.7}$$

Solution of the Navier-Stokes equations formulated in the stream function – vorticity formulation is obtained for the present problem. Navier-Stokes equations in the stream function – vorticity formulation are given as

$$\frac{\partial^2\psi}{\partial x^2}+\frac{\partial^2\psi}{\partial y^2}=-\omega, \tag{3.8}$$

$$\frac{\partial\omega}{\partial t}+u\frac{\partial\omega}{\partial x}+v\frac{\partial\omega}{\partial y}=\frac{1}{Re}\left[\frac{\partial^2\omega}{\partial x^2}+\frac{\partial^2\omega}{\partial y^2}\right]. \tag{3.9}$$

A uniform flow has been prescribed at the inflow boundary AD as shown in Fig. 12(a). Stream function and vorticity values at the remaining boundaries BC, CD and AB are updated using a convective outflow boundary condition [13]. Eqs. (3.8) and (3.9) are non-dimensionalized with respect to free-stream velocity U_∞ as a reference velocity scale and $1/k$ as the time scale. The Reynolds number is defined as $Re=\frac{U_\infty^2}{\nu k}$ [28]. Simulations have been performed for Re=5000, k=50 with a time step of Δt=0.001. The first and the second derivative terms in Eq. (3.9) are evaluated using the coupled compact difference scheme

https://doi.org/10.4208/cicp.101214.250515s Published online by Cambridge University Press

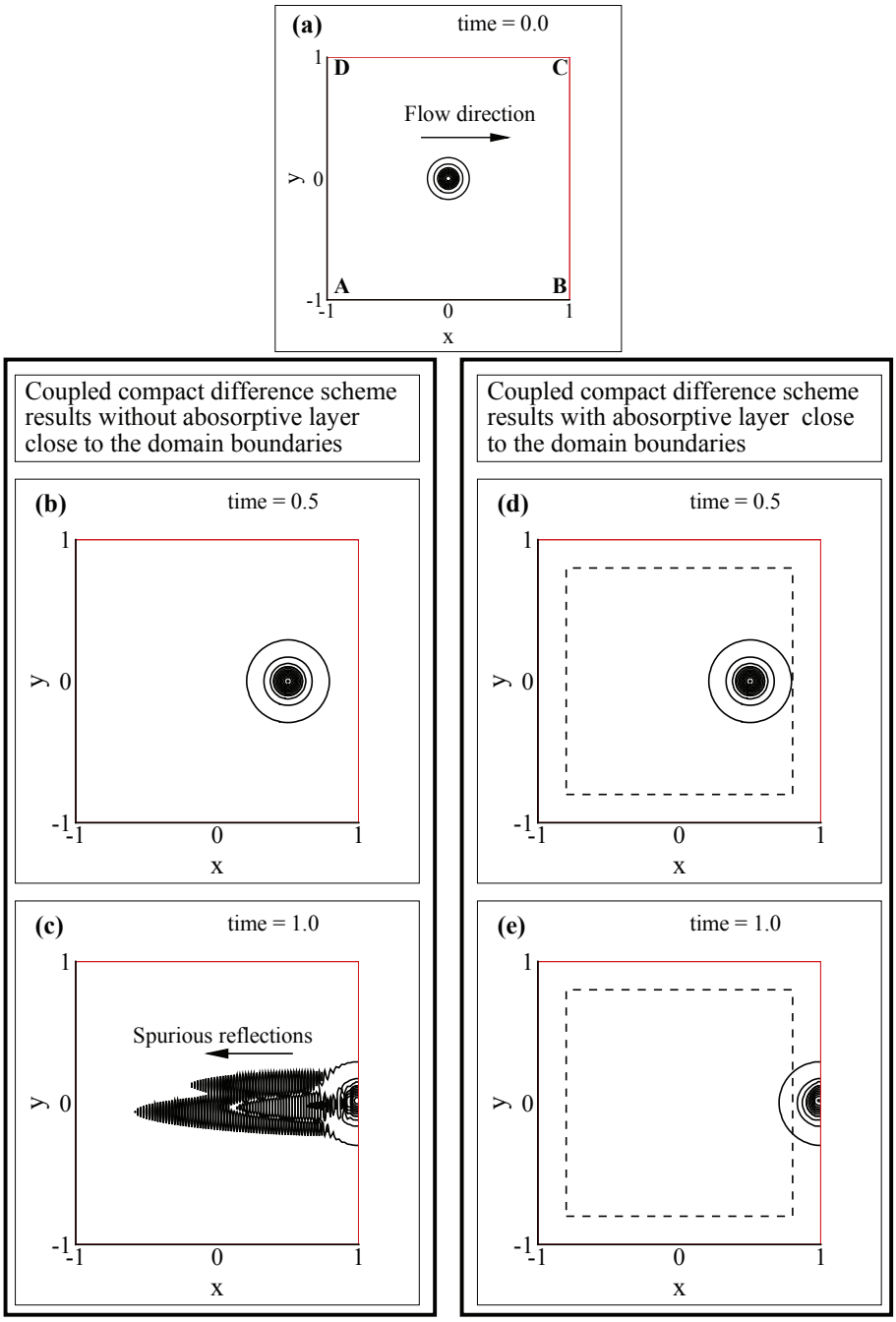


Figure 12: Schematic of the discrete vortex convecting with a uniform flow at the inlet is shown in (a); Spurious reflections are observed from the domain boundaries when the absorbing layer is not prescribed in (c) while these are absent when an absorbing layer with added numerical diffusion (PML technique) is used after the dashed box as shown in (d) and (e).

https://doi.org/10.4208/cicp.101214.250515s Published online by Cambridge University Press

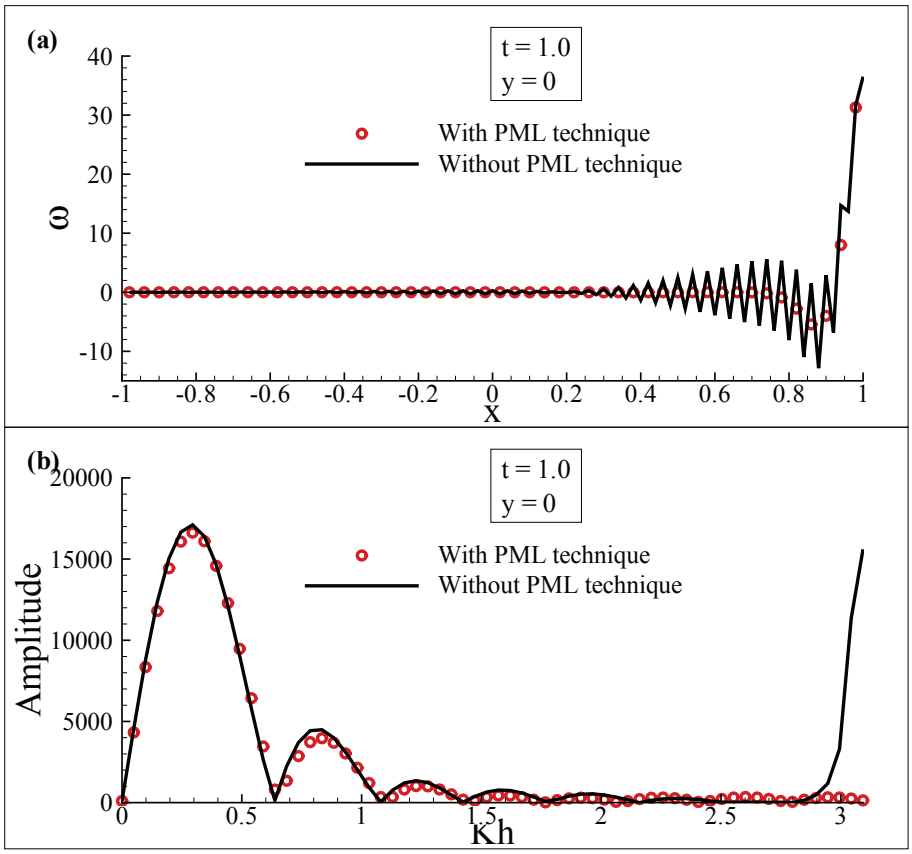


Figure 13: (a) Comparison of the variation of vorticity on the centerline $y=0$ at time $t=1$ in the presence and absence of the PML technique; (b) FFT of the vorticity data in (a) is compared for the results with and without PML. Note the presence of large amplitude of high wavenumber components for the result obtained without PML technique.

while the $CD2$ scheme has been used to discretize stream function Eq. (3.8). Eqs. (3.8) and (3.9) are solved for the given initial condition and the corresponding solutions are shown in the Figs. 12(b) and 12(c), respectively. One observes that the vortex smoothly convects inside the domain however as it reaches the outflow boundary it distorts and spurious components are reflected from the outflow boundary. This is essentially due to the use of inaccurate boundary condition which results in the spurious reflections at the boundary.

Next, we have repeated the same calculation in the presence of an additional absorbing layer close to the domain boundaries marked by the dashed lines in Figs. 12(d) and (e). In the region enclosed by domain boundaries and dashed lines, we have prescribed a diffusion coefficient $\alpha=0.10$. Solution components in this region are heavily damped which has resulted in attenuation of spurious oscillations. Fig. 13(a) shows the variation of vorticity at line $y=0$ at the indicated instant. One observes large high wavenumber fluctuations present in the solution when no absorbing layer technique is used. Corre-

https://doi.org/10.4208/cicp.101214.250515s Published online by Cambridge University Press

sponding FFT also shows rise in amplitude of high wavenumber components for solution obtained without absorbing layer as compared to the solution obtained using absorbing layer. Thus, the coupled compact difference scheme has another important advantage that it can be used as a substitute to the PML technique.

4 Summary and conclusions

Here, we have proposed a new coupled compact difference scheme to evaluate the first, the second and the fourth derivative terms simultaneously. Proposed scheme provides significantly higher spectral resolution while evaluating the first and the higher order derivative terms as shown in Fig. 1. Proposed scheme preserves physical dispersion relation over a considerable wavenumber range when a fourth order four stage Runge-Kutta scheme is used for the time integration as shown by the normalized group velocity contours in Fig. 2(c). Derived scheme shows neutrally stable region in Fig. 2(c) for a small CFL number across a complete wavenumber range when no explicit numerical diffusion is added. Development of a new adaptive methodology for the addition of numerical diffusion is shown for the solution of 1D wave equation in Figs. 6 and 7. This is an important advantage associated with proposed scheme as one is selectively able to damp out the spurious high wavenumber oscillations whenever and wherever it is required to avoid numerical instabilities. Solution obtained using spectrally optimized upwind CCD scheme of [21] shows less accuracy as compared to the proposed scheme in Figs. 8 and 9. Proposed scheme provides accurate results for the model wave equation problems as well as computational acoustic problems as shown in Figs. 10 and 11. In addition to the attractive feature of adaptive diffusion, present scheme also helps to control spurious reflections from the domain boundaries and can be used as an alternate to the perfectly matched layer (PML) technique in Figs. 12 and 13.

References

[1] C. K. W. Tam. *Computational Aeroacoustics a Wave Number Approach*. Cambridge Univ. Press, New York, 2012.
[2] T. Colonius and S. K. Lele. Computational aeroacoustics: progress on nonlinear problems of sound generation. *Prog. Aero. Sciences*, 40:345–416, 2004.
[3] K. Y. Fung, R. S. O. Man, and S. Davis. A compact solution to computational acoustics. *ICASE/LaRC Workshop on Benchmark Problems in Computational Aeroacoustics (CAA)*, pages 59–72, 1995.
[4] P. L. Shah and J. Hardin. Second-order numerical solution of time-dependent, first-order hyperbolic equations. *ICASE/LaRC Workshop on Benchmark Problems in Computational Aeroacoustics (CAA)*, pages 133–141, 1995.
[5] T. K. Sengupta, S. K. Sircar, and A. Dipankar. High accuracy schemes for DNS and acoustics. *J. Sci. Comput.*, 26:151–193, 2006.
[6] L. E. Kinsler, A. R. Frey, A. B. Coppens, and J. V. Sanders. *Fundamentals of Acoustics*. John Wiley & Sons, New York, 2000.

https://doi.org/10.4208/cicp.101214.250515s Published online by Cambridge University Press

[7] T. K. Sengupta, M. K. Rajpoot, S. Saurabh, and V. V. S. N. Vijay. Analysis of anisotropy of numerical wave solutions by high accuracy finite difference methods. *J. Comput. Phys.*, 230:27–60, 2011.
[8] C. Bogey, C. Bailly, and D. Juvé. Noise investigation of a high subsonic, moderate reynolds number jet using a compressible LES. *Theor. Comput. Fluid Dyn.*, 16(4):273–297, 2003.
[9] C.K.W. Tam and Z. Dong. Radiation and outflow boundary conditions for direct computation of acoustic and flow disturbances in a nonuniform mean flow. *J. Comput. Acoustics*, 4 (2):175–201, 1996.
[10] R. Vichnevetsky and J.B. Bowles. *Fourier Analysis of Numerical Approximations of Hyperbolic Equations*. SIAM Stud. Appl. Math., Philadelphia, 1982.
[11] T. Poinsot and D. Veynante. *Theoretical and Numerical Combustion*. R.T. Edwards Inc., 2005.
[12] T. K. Sengupta, A. Dipankar, and P. Sagaut. Error dynamics: Beyond von Neumann analysis. *J. Comput. Phys.*, 226:1211–1218, 2007.
[13] T. K. Sengupta, Y. G. Bhumkar, M. Rajpoot, V. K. Suman, and S. Saurabh. Spurious waves in discrete computation of wave phenomena and flow problems. *App. Math. Comput.*, 218:9035–9065, 2012.
[14] T. K. Sengupta. *High Accuracy Computing Methods: Fluid Flows and Wave Phenomena*. Cambridge University Press., USA, 2013.
[15] C. H. Yu, Y. G. Bhumkar, and T. W. H. Sheu. Dispersion relation preserving combined compact difference schemes for flow problems. *J. Sci. Comput.*, 62(2):482–516, 2015.
[16] Y. G. Bhumkar, T. W. H. Sheu, and T. K. Sengupta. A dispersion relation preserving optimized upwind compact difference scheme for high accuracy flow simulations. *J. Comput. Phys.*, 278:378 – 399, 2014.
[17] T. K. Sengupta, G. Ganeriwal, and S. De. Analysis of central and upwind compact schemes. *J. Comput. Phys.*, 192:677–694, 2003.
[18] M. R. Visbal and D. V. Gaitonde. On the use of higher-order finite-difference schemes on curvilinear and deforming meshes. *J. Comput. Phys.*, 181:155–185, 2002.
[19] S. K. Lele. Compact finite difference schemes with spectral-like resolution. *J. Comput. Phys.*, 103:16–42, 1992.
[20] D. V. Gaitonde, J. S. Shang, and J. L. Young. Practical aspects of higher-order numerical schemes for wave propagation phenomena. *Int. J. Numer. Meth. Eng.*, 45(12):1849–1869, 1999.
[21] P. H. Chiu and Tony W. H. Sheu. On the development of a dispersion-relation-preserving dual-compact upwind scheme for convection-diffusion equation. *J. Comput. Phys.*, 228:3640–3655, 2009.
[22] K. Mahesh. A family of high-order finite difference schemes with good spectral resolution. *J. Comput. Phys.*, 145:332–358, 1998.
[23] T. K. Sengupta, S. Bhaumik, and Y. G. Bhumkar. Direct numerical simulation of two-dimensional wall-bounded turbulent flows from receptivity stage. *Phys. Rev. E*, 85(2):026308, 2012.
[24] Q. Zhou, Z. Yao, F. He, and M. Y. Shen. A new family of high-order compact upwind difference schemes with good spectral resolution. *J. Comput. Phys.*, 227:1306–1339, 2007.
[25] M. K. Rajpoot, T. K. Sengupta, and P. K. Dutt. Optimal time advancing dispersion relation preserving schemes. *J. Comput. Phys.*, 229:3623–3651, 2010.
[26] T. K. Sengupta, Y. Bhumkar, and V. Lakshmanan. Design and analysis of a new filter for LES and DES. *Comput. Struct.*, 87:735–750, 2009.
[27] T. K. Sengupta and Y. G. Bhumkar. New explicit two-dimensional higher order filters. *Comput. Fluids*, 39:1848–1863, 2010.

https://doi.org/10.4208/cicp.101214.250515s Published online by Cambridge University Press

[28] Y. G. Bhumkar. *High Performance Computing of Bypass Transition*. Ph.D. thesis, Department of Aerospace Engineering, Indian Institute of Technology, Kanpur, 2012.
[29] Y. G. Bhumkar and T. K. Sengupta. Adaptive multi-dimensional filters. *Comput. Fluids*, 49, 2011.
[30] T. K. Sengupta, V. V. S. N. Vijay, and S. Bhaumik. Further improvement and analysis of CCD scheme: Dissipation discretization and de-aliasing properties. *J. Comput. Phys.*, 228(17):6150–6168, 2009.
[31] N.D. Sandham, Q. Li, and H.C. Yee. Entropy splitting for high-order numerical simulation of compressible turbulence. *J. Comput. Phys.*, 178(2):307 – 322, 2002.
[32] A. E. Honein and P. Moin. Higher entropy conservation and numerical stability of compressible turbulence simulations. *J. Comput. Phys.*, 201(2):531 – 545, 2004.
[33] B. J. Boersma. A staggered compact finite difference formulation for the compressible Navier-Stokes equations. *J. Comput. Phys.*, 208(2):675 – 690, 2005.
[34] S. Nagarajan, S. K. Lele, and J. H. Ferziger. A robust high-order compact method for large eddy simulation. *J. Comput. Phys.*, 191(2):392 – 419, 2003.
[35] V. Borue and S. A. Orszag. Local energy flux and subgrid-scale statistics in three-dimensional turbulence. *J. Fluid Mech.*, 366:1 – 31, 1998.
[36] N. Haugen and A. Brandenburg. Inertial range scaling in numerical turbulence with hyperviscosity. *Phys. Rev. E*, 70:026405, 2004.
[37] A. G. Lamorgese, D. A. Caughey, and S. B. Pope. Direct numerical simulation of homogeneous turbulence with hyperviscosity. *Phys. Fluids*, 17, 2005.
[38] E. Tadmor. Convergence of spectral methods for nonlinear conservation laws. *SIAM J. Num. Analysis*, 26(1):30–44, 1989.
[39] G-S. Karamanos and G.E. Karniadakis. A spectral vanishing viscosity method for large-eddy simulations. *J. Comput. Phys.*, 163(1):22 – 50, 2000.
[40] R. Pasquetti. Spectral vanishing viscosity method for large-eddy simulation of turbulent flows. *J. Sci. Comput.*, 27:365–375, 2006.
[41] E. Lamballais, V. Fortun, and S. Laizet. Straightforward high-order numerical dissipation via the viscous term for direct and large eddy simulation. *J. Comput. Phys.*, 230(9):3270 – 3275, 2011.
[42] P. C. Chu and C. Fan. A three-point combined compact difference scheme. *J. Comput. Phys.*, 140:370–399, 1998.
[43] H.A.V. der Vorst. Bi-CGSTAB: A fast and smoothly converging variant of Bi-CG for the solution of non-symmetric linear systems. *SIAM J. Sci. Stat. Comput.*, 13:631–644, 1992.
[44] S. I. Green. *Fluid Vortices : Fluid Mechanics and Its Applications*. Springer, 1995.

https://doi.org/10.4208/cicp.101214.250515s Published online by Cambridge University Press